2014 IEEE International Conference on Robotics & Automation (ICRA)
Hong Kong Convention and Exhibition Center
May 31 - June 7, 2014. Hong Kong, China

Force-Based Flexible Path Plans for Robotic Electrode Insertion

Jason Pile, George B. Wanna and Nabil Simaan*

***Abstract*—Rapidly deployable surgical robots pose minimal interruption to surgical workflow and require minimal setup time and equipment to support deployment. This paper explores the concept of rapid deployment through the use of in-vivo sensory information to adapt a pre-operative surgical plan and to increase robustness against registration and misalignment errors during robot deployment. Robotic insertion of cochlear implant electrode arrays is presented as a benchmark application demonstrating this concept. Two key ideas are presented within the context of this application: First, a hybrid position and admittance controller is used to define an insertion path plan that is modified based on in-vivo force measurements in order to reduce sensitivity to misalignment errors. Secondly, a new concept allowing the use of force cues to determine the onset of advance-off stylet electrode array insertion is presented. The new controller is tested with electrode insertions in both plastic models and human cadaveric specimens. The experiments show that insertion forces may be maintained or reduced compared to preplanned trajectories relying solely on the initial registration.**

I. Introduction

Surgical robots augment surgeon's capabilities by providing distal dexterity enhancement [1]–[3] and precision enhancement [4], [5]. The added capabilities offered by surgical robots are typically justified when they act as technological enablers (i.e. when they enable surgeons to carry tasks that would have been otherwise impossible to perform) and when there is a clear patient benefit and an economic justification to the added cost. Clinically successful systems must overcome impediments to technology adoption by minimizing their impact in terms of size, cost, footprint in the surgical arena, and interruption/delays to the existing non-robot-assisted surgical workflow. In this paper, we focus on reducing surgical deployment time and cost by eliminating the need for costly imaging technology and exact registration to the anatomy.

This paper focuses on automated electrode array insertion for cochlear implant (CI) surgery. CI surgery introduces an implant into the cochlea to restore acoustic perception in patients with profound or total hearing loss through direct electrical stimulation. This application demonstrates our proposed rapid deployment approach, which leverages surgeon expertise and in-vivo sensory information to adapt the electrode insertion. Surgeon expertise assumes fundamental understanding of the cochlear anatomy and in-vivo sensory information includes position of the electrode array tip, estimates of the electrode array shape, and measured insertion forces.

The topics most related to the subject matter of this paper include works on robotic insertion of flexible beams and works on electrode array insertion for cochlear implant surgery. Works on flexible beam insertion typically assume knowledge of the beam kinematics, known hole geometry, and beam shape estimation with mechanics models or through vision systems [6]–[8]. In this work, we are inspired by these approaches but we do not make direct use of these results due to several limitations: the electrode arrays are under-actuated composite beams, the application domain does not allow 3D vision systems to confirm the electrode shape, and the location and shape of the target hole are not precisely known.

The first work on robotic insertion of electrode arrays appeared in [9], [10] where different kinematic arrangements and degrees of freedom in manipulating electrode arrays during the insertion process were considered. Subsequent works including [11], [12] have presented clinically adapted versions of electrode array insertion tools. There is also work focused on robotic drilling of the mastoidectomy [13], [14] and drilling access to the cochlea [15] for percutaneous insertion [11], [12], [16]. So far in the works on insertion systems, many use force sensing as a metric for insertion quality [9], [11], [17]–[22] but, to the best of the authors' knowledge, there has been no exploration of using force based control methods to actively adapt electrode insertion plans.

Our prior work [23] presented an insertion plan based solely on kinematic modeling of the electrode arrays and perfect knowledge of the cochlea shape. The results of this insertion planner were in close agreement with manufacturer specification for recommended manual insertion technique. However, it is unlikely that a deployed robotic system will have both perfect knowledge of the cochlea shape and perfect registration to the anatomy since the entrance into the cochlea is created intra-operatively. Methods of completing implant insertion without reliance on extra sensors and imaging steps also has the potential to save cost and time.

In this work, we investigate the potential application of hybrid position/admittance control to the insertion of cochlear implant electrodes. The clinical goal is to move toward rapidly deployable robotic insertion tools that are not constrained to fixed registration techniques or require additional new components outside the robot itself to perform the task. Validation of this approach is presented through testing in plastic models and cadaveric specimens.

II. Surgical Environment

A. Cochlear Anatomy

The cochlea is a structure in the inner ear where acoustic energy is converted to electrical impulses for processing in the brain as sound. It is a helical structure consistent of three helical chambers; the scala tympani, the scala media, and the

This work was supported by Cochlear Corporation LTD

J. Pile and N. Simaan are with the Department of Mechanical Engineering, Vanderbilt University, Nashville, TN 37212, USA.

G. Wanna is with the Department of Otolaryngology, Vanderbilt University, Nashville, TN 37212, USA.

* corresponding author.

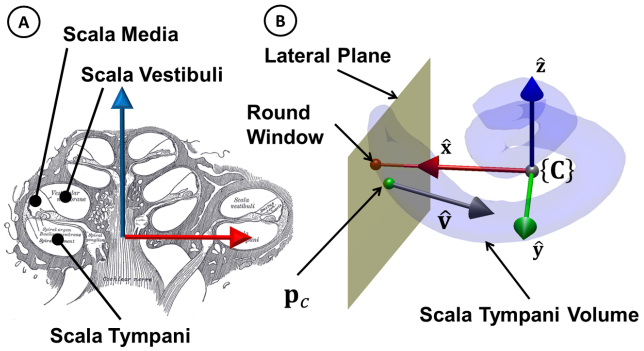

Fig. 1. Cochlea coordinate frame. (A) Internal cross section of the cochlea; the top chamber is the scala vestibuli and lower chamber is the scala tympani. (B) The frame C is define with $\hat{\mathbf{z}}$ colinear with the cochlea's helical axis and $\hat{\mathbf{x}}$ passing through the center of the round window. The point $\mathbf{p}_c$ is the location of the surgeon-created entrance into the cochlea. In the case of a round window insertion $\mathbf{p}_c$ lies along $\hat{\mathbf{x}}$.

scala vestibuli (Fig. 1(A)). The scala tympani is separated from the scala media by a thin *basilar membrane*.

During CI surgery, electrode arrays are inserted into the scala tympani since insertion in this chamber has been shown to be advantageous [24]. The round window is a visible anatomical landmark that seals the base of the scala tympani with a thin membrane. The electrode array is inserted into the scala tympani by using either the round window or by surgically creating a new opening called a *cochleostomy*, which is typically located inferior to the round window [25]. In the following analysis, we use the term *insertion point* to refer to either the cochleostomy or the round window - depending on the technique practiced by the surgeon.

To perform robotic insertion of cochlear implants a set of frames must be defined to describe the spatial relationship between the robot, electrode, and the cochlea itself. Recently, a panel of clinicians have proposed a standardized coordinate frame model for the cochlea [26], which is adopted here to define the cochlea frame $\{\mathbf{C}\}$. Figure 1(B) depicts frame $\{\mathbf{C}\}$ with respect to cochlea features. The axis of the cochlea's helix defines ${}^{C}\hat{\mathbf{z}}$ with the axis ${}^{C}\hat{\mathbf{x}}$ passing through the center of round window.

B. Electrode arrays

CI electrode arrays fall into two major categories based on their desired location inside the cochlea. Lateral wall electrode arrays (LEA) are thin, straight electrodes designed to slide along the lateral (outer) wall of the cochlea. Perimodiolar electrode arrays (PEA's) are under-actuated, flexible structures designed to remain in close proximity of the modiolar (inner) wall of the cochlea. In both electrode designs there is a desire to produce atraumatic insertions through a combination of compliant mechanical design and soft surgical technique [27]. Also, when using either electrode design the goal for final placement is to remain in the scala tympani and not puncture the basilar membrane to avoid trauma to ganglion cells which support residual hearing. PEA's use a *stylet* to straighten a

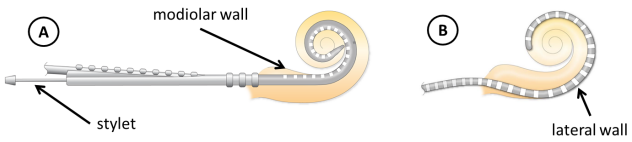

Fig. 2. CI electrode arrays. (A) Perimodiolar electrode arrays (Cochlear Contour Advance shown) are single DoF flexible structures designed to maintain contact with the modiolus of the cochlea. They are actuated through the removal of an embedded stylet. (B) Lateral wall electrodes are non-actuated and designed to maintain contact with the outer wall of the cochlea.

coiled elastomeric electrode array. The stylet is initially fully inserted in the electrode array and is removed from the PEA as it is inserted into the cochlea using a technique called *AOS* (advance off stylet). This technque allows the PEA to conform to the shape of the inner wall during insertion [27]. For this study, PEA were used due to the extra DoF provided by the under-actuated electrode design.

C. Surgical Work-flow and Relevance

We briefly review the standard flow of CI surgery to provide context to where robotic insertion fits into the framework and its potential benefits. Imaging is routinely used in the preoperative planning stage to alert the surgeon to anatomical structures they wish to avoid damaging during drilling. At the start of the procedure the surgeon gains access to the inner ear through a mastoidectomy and excavation of bone leading to the facial recess. After opening the facial recess the surgeon has a direct view of the cochlea and can identify the round window. The surgeon selects the point of entry into the cochlea and creates an opening approximately $1mm$ in diameter. The implant's transceiver is fixed to the patient's skull and then the implant is gently inserted into the cochlea. After testing the implant's basic electric function the surgical site is closed.

When using a robot for electrode insertion we assume that the patient's skull can be held fixed to the operative table using head straps and Mayfield frames that lock on the patient's teeth. We assume that the surgeon knows the location of the electrode insertion point and can use the robot to digitize the location of this point. We also assume that the intra-cochlear anatomy is devoid of abnormalities as can be verified by routine pre-operative imaging required by the current surgical workflow. If 3D exact reconstruction and segmentation methods are used as described in [28] then a more exact model of the intracochlear anatomy may be used. In the absence of an exact intracochlear model we assume that the general intracochlear anatomy follows the a shape function proposed by Cohen et al. [29]. Since our approach relies on using force insertion data to modify the insertion path, we do not depend on exact knowledge of the intra-cochlear anatomy.

The proposed robotic insertion algorithm and workflow incorporates both a preplanning phase and a hybrid admittance controller to compensate for registration errors during insertion. The steps for insertion are defined as follows:

1) The surgeon directs the tip of the robot gripper to the insertion point and defines the suggested angle of

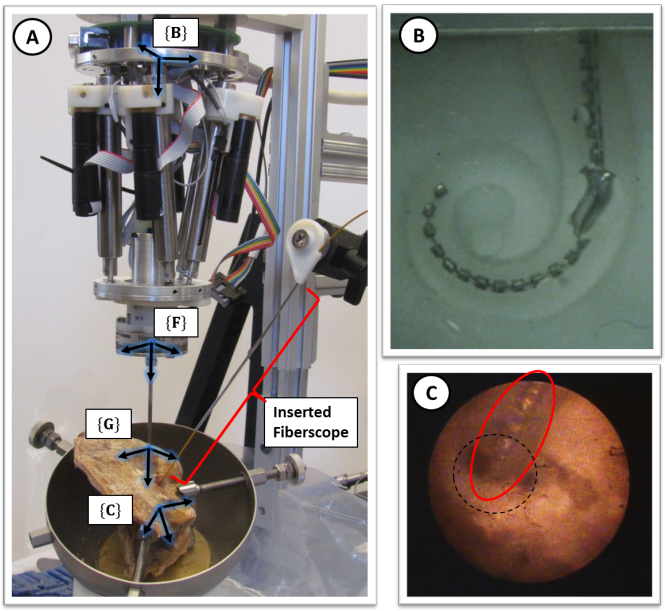

Fig. 3. Robotic cochlear implant insertion system. (A) The system is shown prior to insertion in a cadaveric temporal bone specimen. Approximate location of the relevant coordinate frame are overlayed. (B) Image of electrode placement taken in the plastic phantom model. (C) a fiberscope inserted through the excavated ear canal was used to observe electrode insertion (solid circle) into the human cochlea (dashed circle)

approach. This defines the final point of the preplanned insertion.

2) After retracting the robot tip from the insertion point, the PEA is loaded into the gripper and the force sensor goes through an unbiasing routine.
3) The surgeon directs the robot to bring the tip of the electrode to the insertion point.
4) An estimate of the initial shape of the PEA is made and the insertion planning algorithm from [23] generates a nominal insertion path.
5) The hybrid position-admittance control laws are enabled and the insertion is executed.

Sections III and IV present the details of the insertion planning and proposed insertion strategy.

III. Robotic Registration and Insertion

The experimental setup for the robotic insertion system is shown in Fig. 3. Frame $\{\mathbf{B}\}$ is used to designate the robot base frame, which is held at a fixed position and orientation relative to $\{\mathbf{C}\}$[1] - the patient's cochlea frame. The location of the insertion point is denoted by the vector $\mathbf{p}_c$ and the insertion direction by unit vector $\hat{\mathbf{v}}$. The PEA frame $\{\mathbf{E}\}$ is coincident with the end effector gripper frame $\{\mathbf{G}\}$ and the gripper position and orientation are parameterized by $\mathbf{x}$ and ϕ respectively.

The shape of the electrode array (in the absence of outside forces) is constrained to a plane in frame $\{\mathbf{C}\}$ and whose local

[1]All vector quantities, unless explicitly expressed in another frame, can be assumed to be represented in frame $\{\mathbf{B}\}$

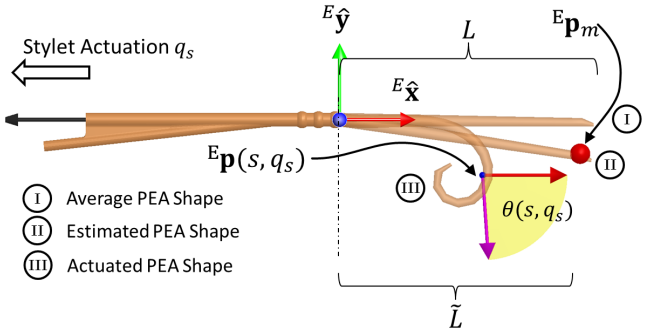

Fig. 4. PEA shape estimation. The shape is defined by the tangent $\theta(s, q_s)$ of the PEA's modiolar edge. A nominal PEA shape $\bar{\theta}(s, q_s)$ (I) is modified to pass through the known point of insertion, ${}^E\mathbf{p}_m$ (II). The distance along the PEA curve to the insertion point is denoted as $\tilde{L}$. An estimate of the relationship between $\dot{\theta}$ and stylet actuation $\dot{q}_s$ completes the kinematic model of the PEA with a example of an actuated PEA shown with (III).

tangent can be written as a function $\theta(s, q_s)$ where s represents arc length and q_s is the length of removed stylet. A simple monomial basis functions ($\boldsymbol{\psi}(s)$ and $\boldsymbol{\eta}(q_s)$) in terms for arc length $s \in [0, L]$ and stylet actuation q_s are used to provide a modal representation for the natural PEA shape.

$$\boldsymbol{\psi}(s) = [s^0, s^1, s^2, ..., s^{n-1}]^T \tag{1}$$

$$\boldsymbol{\eta}(q_s) = [q_s^0, q_s^1, q_s^2, ..., q_s^{m-1}]^T \tag{2}$$

From prior measurements on PEA shapes [23], third order polynomials were sufficient to accurately capture the PEA kinematics ($m = n = 4$). Using a calibration matrix $\mathbf{A} \in \mathbb{R}^{m \times n}$, obtained experimentally [9], [23], the local tangent along the modiolar side of the PEA is used to describe the shape of the PEA:

$$\theta(s, q_s) = \boldsymbol{\psi}(s)^T \mathbf{A} \boldsymbol{\eta}(q_s) \tag{3}$$

The position of points ${}^E\mathbf{p}$ of the electrode array is given by the integral along its tangent:

$${}^E\mathbf{p}(s, q_s) = \left[\int_0^s c(\theta(\tau, q_s))\, d\tau, \quad \int_0^s s(\theta(\tau, q_s))\, d\tau, \quad 0 \right]^T \tag{4}$$

where $c(\cdot)$ and $s(\cdot)$ designate the cosine and sine functions.

Calibration of individual PEA's prior to insertion is not clinically viable since reinsertion of the stylet into an array is not allowed prior to insertion in a patient. However, prior measured data may be used to construct a likely PEA matrix $\mathbf{A}$.

Figure. 4 is used to describe the insertion constraint. When the PEA tip is brought to the insertion point it must pass through $\mathbf{p}_c$. We define the point ${}^E\mathbf{p}_m$ as a measured point along the PEA length in frame $\{E\}$ with[2] $\mathbf{p}_m = {}^E\mathbf{T}_B \mathbf{p}_e$. The location of the proximal end of the PEA is also known to be coincident with the origin of frame $\{E\}$.

Creating an estimate of the calibration matrix $\mathbf{A}$ is a two step process: first the initial shape is defined and then the

[2]Notation ${}^B\mathbf{T}_A$ is the homogeneous transformation of frame $\{A\}$ as expressed in frame$\{B\}$

relationship between stylet actuation and change in shape is applied. Data from previously calibrated PEA's is used to generate an estimation for the current PEA. The calibration matrix can be split into a column vector and a 4×3 matrix:

$$\mathbf{A} = \begin{bmatrix} \mathbf{a}_{0_{[4\times1]}}, & \tilde{\mathbf{A}}_{[4\times3]} \end{bmatrix} \tag{5}$$

When $q_s = 0$, (3) can be written as:

$$\theta(s,0) = \boldsymbol{\psi}(s)^T \mathbf{a}_0 \tag{6}$$

We define the average initial PEA shape as $\bar{\theta}(s,0)$ and discretize the PEA into z evenly distributed points to create the vector $\bar{\boldsymbol{\theta}} \in \mathbb{R}^{z\times1}$. For a given $\mathbf{a}_0$, a set of discretized points of the estimated shape creates the vector $\tilde{\boldsymbol{\theta}} \in \mathbb{R}^{z\times1}$. The difference between the average and estimated shape is then defined as:

$$\Delta\boldsymbol{\theta} = \tilde{\boldsymbol{\theta}} - \bar{\boldsymbol{\theta}}\,(s,0) \tag{7}$$

The scalar value $\tilde{L} \in [0, L]$ defines a point along the PEA which intersects with the insertion point ${}^E\mathbf{p}_m$. Using these definitions, the initial shape of the PEA is estimated by numerically solving the following constrained optimization problem:

$$\begin{aligned} &\underset{\mathbf{a}_0,\tilde{L}}{\text{minimize}} \quad \Delta\boldsymbol{\theta}^T\Delta\boldsymbol{\theta} \\ &\text{subject to} \quad \mathbf{p}(\tilde{L},0) = \mathbf{p}_m, \quad \tilde{L} \in [0,L] \end{aligned} \tag{8}$$

The solution set of coefficients are denoted as $\tilde{\mathbf{a}}_{0,est}$. Once the estimate of the initial shape ($\theta(s,0) \forall s \in [0,L]$) is made, an estimate of the average rate of change of PEA shape to stylet actuation ($\frac{d\bar{\theta}}{dq_s}$) is based on the average of rates of change of previously calibrated PEA's [23]. It can be shown that the average of the h known calibration matrices $\tilde{\mathbf{A}}_i, i = 1, ..., h$ describes the average rate of shape rate per stylet pull $\frac{d\bar{\theta}}{dq_s}$ and the estimated calibration matrix becomes:

$$\mathbf{A}_{est} = \begin{bmatrix} \mathbf{a}_{0,est} & \sum_{i=1}^{h} \frac{1}{h}\tilde{\mathbf{A}}_i \end{bmatrix} \tag{9}$$

After estimating the calibration matrix $\mathbf{A}_{est}$, the insertion path is calculated as a function of insertion depth d as presented in [23]. In this paper this precalculated insertion path is defined as $\mathbf{x}_p(d)$ and $q_s(d)$. During insertion, this path is modified by the hybrid position-admittance controller.

IV. Hybrid Position-Admittance Controller

The goal of the hybrid position-admittance controller is to correct for both registration and shape estimation errors during insertion. This type of controller is similar to hybrid force controllers that have been applied to many problems and the foundational work can be reviewed in [30], [31]. Figure 5 shows a simplified block diagram of the implemented controller. The original point commanded from the insertion trajectory $\mathbf{x}_p(d)$ is called $\mathbf{x}_{des}$ to which the force controller adds a corrective value $\mathbf{x}_{admit}$ to send as the commanded position to the low level controller (LLC) as $\mathbf{x}_{ref}$. The LLC contains the standard task space controller calculating inverse kinematics and using a PID controller for joint level control.

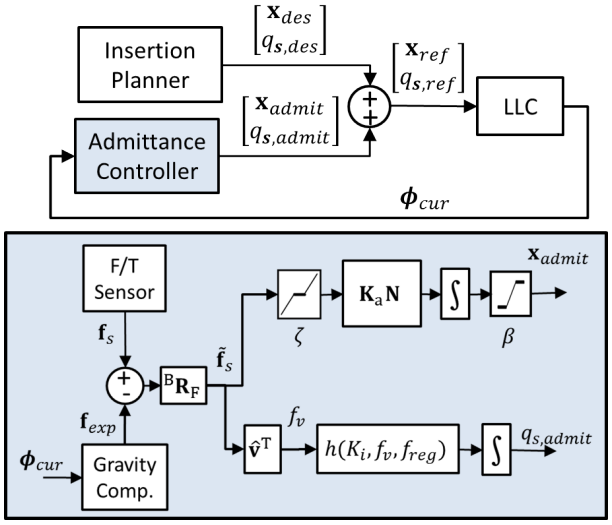

Fig. 5. Hybrid Position-Admittance Controller. Forces acting in the space of $\mathbf{N}$, which defines the lateral plane, apply corrective displacement on the command position $\mathbf{x}_{des}$. The values ζ and β define the deadband and saturation boundaries respectively. Force acting along $\hat{\mathbf{v}}$ affects the rate of stylet actuation $\dot{q}_s$. The function $h(f_v,\ f_{reg})$ refers to (17). The low level controller (LLC) controls the end effector position. Orientation $\boldsymbol{\phi}$ is not affected by the admittance law and is omitted in areas for clarity

The force/moment sensor frame is denoted as $\{F\}$ and the force applied to the sensor is $\mathbf{f}_s^T$. Force measurements are used to modify control in the lateral plane of insertion and separately for the actuation of the stylet.

A. Hybrid Controller in Lateral Plane

Given $\hat{\mathbf{v}}$ as the insertion direction in the robot base frame we wish to actively adjust the end effector position in the plane normal to $\hat{\mathbf{v}}$ based on perceived forces in that plane. A projection matrix $\mathbf{N}$ is defined as:

$$\mathbf{N} = \mathbf{I} - \hat{\mathbf{v}}\left(\hat{\mathbf{v}}^T\hat{\mathbf{v}}\right)^{-1}\hat{\mathbf{v}}^T \tag{10}$$

which governs the space in which our force control can act. Forces acting in the space of $\mathbf{N}$ are called lateral forces. The perceived force (${}^F\mathbf{f}_s$) requires a forward feeding compensation term ${}^F\mathbf{f}_e(\boldsymbol{\psi})$ to account for the force due to gravity acting on the insertion module:

$$\mathbf{f}_e(\boldsymbol{\phi}) = {}^F\mathbf{R}_B(\boldsymbol{\phi})\mathbf{f}_g + \mathbf{b}_f \tag{11}$$

where $\mathbf{f}_g$ is the gravitational load, $\mathbf{b}_f$ is the force sensor bias and ${}^F\mathbf{R}_B$ is the rotation matrix describing frame $\{B\}$ in frame $\{F\}$. Each time the system is initialized a training routine is performed to determine the direction of gravity and the sensor's static bias. This training requires collecting a set of poses varying in orientation and applying a least squares fitting to $\mathbf{f}_g$ and $\mathbf{b}_f$ in (11).

After applying a $25ms$ moving average filter at $1kHz$ sampling rate and unbiasing, the resulting force projection into the robot base frame is denoted as $\tilde{\mathbf{f}}_s$ where:

$$\tilde{\mathbf{f}}_s = {}^B\mathbf{R}_F\left({}^F\mathbf{f}_s - {}^F\,\mathbf{f}_e(\boldsymbol{\phi})\right) \tag{12}$$

The gravity load compensation has a residual amount of force depending on tool orientation which should not be allowed to influence the controller. A deadband margin ζ is applied to the force reading $\tilde{\mathbf{f}}_s$ and the resulting signal is denoted as $\bar{\mathbf{f}}_s$. The admittance control law is a proportional gain $\mathbf{K}_a$ which applies corrective action $\Delta\mathbf{x}$ to the nominal insertion path $\mathbf{x}_p(d)$.

$$\dot{\mathbf{x}}_{admit} = \mathbf{K}_a \mathbf{N} \bar{\mathbf{f}}_s \tag{13}$$

The corrective action $\dot{\mathbf{x}}_{admit}$ is limited by a displacement saturation value β such that:

$$\left\| \int_0^t \dot{\mathbf{x}}_{admit} dt \right\| \leq \beta \tag{14}$$

This saturation limit acts as a safety against potential malfunctioning in the force transducer.

B. Underactuated Electrode Controller

Insertion direction forces are primarily governed by proper execution of AOS technique. The actuation of the stylet is unidirectional ($\dot{q}_s \geq 0$). In an ideal PEA insertion, the electrode is inserted until the basal turn, at which point the surgeon holds the stylet fixed in space and continues to guide the rest of the electrode into the cochlea. If done correctly, the PEA maintains minimal sliding contact with the modiolar wall and does not touch the lateral wall (Fig 2(A)). Forces along the insertion direction $\hat{\mathbf{v}}$ are called insertion forces (f_v) defined as:

$$f_v = \hat{\mathbf{v}}^T \tilde{f}_s \tag{15}$$

If the AOS techique is executed too late, the PEA will make contact with the lateral wall and the reaction force may be detected along the insertion vector. Actuation of the stylet moves the PEA toward the modiolar wall and in general establishes a relationship of the form:

$$\dot{q}_s = g(d)\dot{f}_v, \ \forall \dot{q}_s \geq 0 \tag{16}$$

The exact form of $g(d)$ depends on the internal geometry of the cochlea, the elastic properties of a specific PEA, and the lubrication in the cochlea. A simple approach for online applications is to take a look at the general mechanics of the insertion and attempt to use $\dot{q}_s$ to regulate insertion force $\tilde{f}_v$. No significant force can be imparted on the cochlea in the insertion direction $\hat{\mathbf{v}}$ by the PEA until the electrode has passed the first turn. In some experiments [11], [17] it can be seen from the data that the PEA can reverse the direction of force and effectively pull itself into the cochlea. We propose using a control law on stylet actuation of the form:

$$\dot{q}_{s,admit} = h\left(K_i, f_v, f_{reg}\right) = K_i \frac{\gamma(d)}{2}\left[f_{reg} - \tilde{f}_v + \left\| f_{reg} - \tilde{f}_v \right\|\right] \tag{17}$$

where f_{reg} is a limit to the expected insertion force (a negative value for resistance to insertion), K_i is a proportional gain in units of mm/Ns, and $\gamma(d)$ that controls when adjustment to AOS is used. We define γ_1 and γ_2 as the lower and upper bounds for insertion depth d thats corresponds to onset of AOS insertion technique. Using these definitions, $\gamma(d)$ is given by:

$$\gamma(d) = \begin{cases} 0, & d \leq \gamma_1 \\ \frac{d-\gamma_1}{\gamma_2-\gamma_1}, & \gamma_1 < d < \gamma_2 \\ 1, & d \geq \gamma_2 \end{cases} \tag{18}$$

The control law results in no correcting action to the pre-planned stylet actuation for forces greater than f_{reg} and is a proportional adjustment for large resistive insertion forces. The total adjustment to the stylet actuation is $q_{s,admit}$ where:

$$q_{s,admit} = \int_0^t \dot{q}_{s,admit} dt \tag{19}$$

and is applied to the original desired stylet actuation $q_{s,des}$ as shown in Fig. 5. The total retraction of the stylet is limited to 15mm since displacement beyond this point no longer affects the shape of the PEA.

TABLE I
SUMMARY OF EXPERIMENT TRIALS

Set	Model	N	K_a (mm/Ns)	K_i (mm/Ns)	$[\gamma_1, \gamma_2]$ (mm)
0 [21]	plastic	95	0	0	N/A
0b [21]	cadaveric	8	0	0	N/A
1	plastic	5	20	0	N/A
2	plastic	5	50	0	N/A
3	plastic	5	50	50	[4, 7]
4	plastic	5	50	80	[4, 7]
5	cadaveric	5	50	80	[4, 7]

V. EXPERIMENTAL EVALUATION

The proposed insertion control law was validated through a series of insertions in both plastic phantom models and in human cadaveric temporal bone specimens. Insertions in plastic models provided a means of observing electrode behavior during insertion while temporal bone experiments determined whether benefits in force reduction translate to real patient anatomy.

Table I summarizes the experimental parameters. Data from prior insertions [21] act as a baseline for comparison as they did not use force control and relied solely on pre-registration. The data sets "0" and "0b" reference plastic and bone insertions respectively. The value of N indicates the number of separate insertions in the data set. Only lateral admittance control was applied to sets 1 and 2 at different proportional gains. Force based adjustment of the AOS technique was then added in sets 3 and 4 with insertion in temporal bone occurring in set 5.

A 6 DoF Stewart-Gough parallel robot, previously presented in [32] was used to control the end effector holding the PEA called the insertion module (Fig. 3) shown in [21]. An ATI Industrial Nano 43 transducer with a force resolution of $0.004N$ and sampling rate of 1kHz was used to measure forces. The entire system was controlled using the MATLAB xPC real time control software on a 500MHz target machine (Advantech pc\104 single board computer).

TABLE II
FORCE RESULTS BETWEEN CASES

Specimen Type	Plastic Phantom					Cadaveric	
Set	0	1	2	3	4	0b	5
Insertion Force (N)	0.042 (0.023)	0.052 (0.029)	0.062 (0.034)	0.037 (0.018)	0.044 (0.021)	0.071 (0.033)	0.046 (0.005)
t-test (p)	N/A	0.090	0.032	0.325	0.722	N/A	0.033
Post-AOS Ins. Force (N)	0.047 (0.028)	0.076 (0.042)	0.091 (0.041)	0.050 (0.023)	0.056 (0.036)	0.110 (0.058)	0.051 (0.021)
t-test (p)	N/A	0.085	0.008	0.584	0.482	N/A	0.009
Peak Ins. Force (N)	0.190	0.186	0.168	0.124	0.134	0.284	0.143
Lateral Force (N)	0.016 (0.016)	0.022 (0.014)	0.026 (0.013)	0.018 (0.014)	0.024 (0.018)	0.026 (0.030)	0.031(0.023)

Experiments for unbiasing the force sensor according to (11) resulted in a residual force with magnitudes below $0.03N$. Accordingly, we have set the deadband margin $\zeta = 0.03N$. The saturation boundary for the lateral admittance controller was set to $\beta = 5mm$ as used in (14).

The insertion procedure for the plastic and cadaveric specimens were identical. The cochlea was lubricated with a 50% water / glycol solution as demonstrated in [17], [33] for the plastic model and no additional lubricant was applied to the temporal bone specimen as a fresh cochlea was used. The steps presented in Section II-C were followed for insertion. A Phantom Omni haptic control system was used to teleoperate both the gripper tip and PEA distal tip to the insertion point. The ear canal was opened to provide fiberscope access to view the entire insertion into the cochlea. After completing the insertion, the electrode was extracted and data collected by the real time control system was exported for processing. The multimedia extension shows an insertion experiment with force data and an example of the modeled PEA kinematics.

VI. RESULTS AND DISCUSSION

Table II provides a summary of the insertion force results across all sets. Force values are presented as averages with the standard deviation in parentheses. Figures 6 and 7 plot the average force in the insertion direction for the plastic and bone insertion cases respectively. The percentage of insertion completed based on distance travelled through the insertion is parameterized by λ and uses data from the first 95% of the insertion process. This is due to registration error causing gripper collision with the insertion point. These contact forces are significantly higher than the intra-cochlear forces from insertion and do not represent legitimate intra-cochlear forces. While collisions at the end of insertion were small in number, a range of 95% was applied to all insertions to provide a fair comparison.

Insertion forces were broken into two subsets; across the entire insertion and during the AOS portion of insertion. Admittance control applied in the lateral plane is active through the entire insertion while the stylet actuation admittance control can only affect the AOS portion of insertion. Set 0 and 0b act as the baseline for comparison for plastic and bone insertions respectively. A single sided t-test was used to compare the new insertion controller's performance with previous data. Set 2 showed a statistically significant increase in average force compared to Set 0 ($p = 0.032$ for full insertion and $p = 0.008$ post-AOS). However in sets 3 and 4, which show

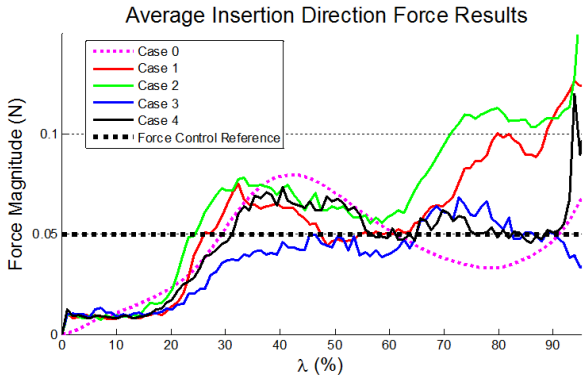

Fig. 6. Average Insertion Force Data for Plastic Model Insertions

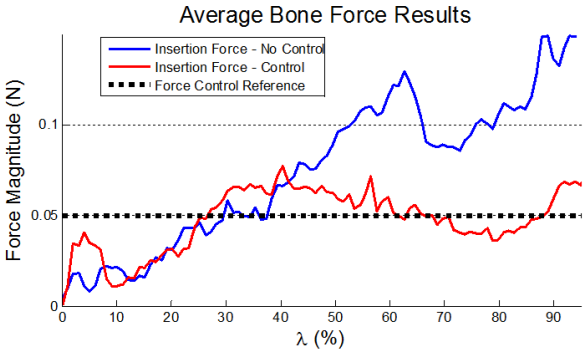

Fig. 7. Average Bone Insertion Forces

enabled stylet admittance control data, there was no difference with the baseline set and peak forces were also reduced. The bone insertion data shows a statistical difference in post-AOS insertion force in the temporal bone insertions when using the admittance control law compared to non-force guided AOS from our prior study [21]. There was no significant different in lateral force between the sets. Little change in average pre-AOS insertion forces could be seen.

Figure 8 shows final corrections to insertion point location in the lateral plane at the end of insertion. In some cases, the initial registration error was higher than one diameter of the PEA. The force controller sufficiently corrected the error without large changes in insertion force. The entrance into the cochlea requires passing through the facial recess and motion corrections much greater than $\pm 2mm$ are not generally possible due to anatomical restrictions.

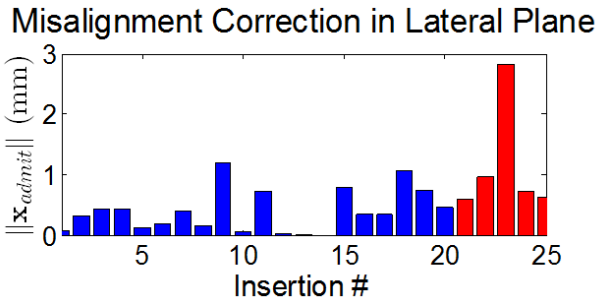

Fig. 8. Correction to insertion point registration applied by hybrid force controller. Insertions 1 - 20 from plastic model sets and 21-25 are corrections in bone insertions.

VII. Conclusions

In this work a hybrid force-position controller was applied to the insertion of perimodiolar cochlear implants in both plastic models and cadaveric specimens. The controller was capable of maintaining insertion forces equivalent to those previously observed using rigid registration fixtures. In some cases the initial registration of the insertion point was greater than one PEA diameter and lateral forces could be maintained below 30mN. Forces in temporal bone insertions saw a statistically significant reduction in insertion force when applying the hybrid force control. The process described in this work still requires a visually guided estimate of the insertion point location and further effort will be placed on removing this step through integrated vision and elastic modelling of the electrode array.

References

[1] S. Charles, "Dexterity Enhancement for Surgery," in *Computer-integrated surgery*, R. H. Taylor et al., Ed. Cambridge, MA: MIT Press, 1996, pp. 467–472.

[2] G. Guthart and J. Salisbury, "The Intuitive/sup TM/ telesurgery system: overview and application," in *Proc. 2000 IEEE Int. Conf. Robotics and Automation*, vol. 1. IEEE, 2000, pp. 618–621.

[3] N. Simaan et al., "A dexterous system for laryngeal surgery," in *Proc. 2004 IEEE Int. Conf. Robotics and Automation*. New Orleans: IEEE, 2004, pp. 351–357 Vol.1.

[4] R. Taylor, "A Steady-Hand Robotic System for Microsurgical Augmentation," *The Int. J. of Robotics Research*, vol. 18, no. 12, pp. 1201–1210, Dec. 1999.

[5] A. Wei Tech et al., "An intelligent hand-held microsurgical instrument for improved accuracy," in *2001 Conf. Proc. of the 23rd Ann. Int. Conf. of the IEEE Eng. in Medicine and Biology Society*, vol. 4. Istanbul, Turkey: IEEE, 2001, pp. 3450–3453.

[6] Z. Liu and T. Nakamura, "Learning Insertion Task of a Flexible Beam by Virtual Agents," 2002, pp. 3290–3295.

[7] H. Nakagaki et al., "Study of deformation and insertion tasks of a flexible wire," in *Proc. 1997 IEEE Int. Conf. Robotics and Automation*, vol. 3, no. April. IEEE, 1997, pp. 2397–2402.

[8] W. Kraus and B. McCarragher, "Case studies in the manipulation of flexible parts using a hybrid position/force approach," in *Proc. 1997 IEEE Int. Conf. Robotics and Automation*, vol. 1, no. April. IEEE, 1997, pp. 367–372.

[9] J. Zhang et al., "A pilot study of robot-assisted cochlear implant surgery using steerable electrode arrays." *MICCAI*, vol. 9, no. Pt 1, pp. 33–40, Jan. 2006.

[10] J. Zhang et al, "Optimal Path Planning for Robotic Insertion of Steerable Electrode Arrays in Cochlear Implant Surgery," *J. of Medical Devices*, vol. 3, no. 1, p. 011001, 2009.

[11] D. Schurzig et al., "Force of cochlear implant electrode insertion performed by a robotic insertion tool: comparison of traditional versus Advance Off-Stylet techniques." *Otology & neurotology*, vol. 31, no. 8, pp. 1207–10, Oct. 2010.

[12] O. Majdani et al., "Force measurement of insertion of cochlear implant electrode arrays in vitro: comparison of surgeon to automated insertion tool." *Acta oto-laryngologica*, vol. 130, no. 1, pp. 31–6, Jan. 2010.

[13] H. Lim et al., "Image-guided robotic mastoidectomy using human-robot collaboration control," *2011 IEEE Int. Conf. on Mechatronics and Automation*, pp. 549–554, Aug. 2011.

[14] T. Klenzner et al., "New strategies for high precision surgery of the temporal bone using a robotic approach for cochlear implantation." *European archives of oto-rhino-laryngology*, vol. 266, no. 7, pp. 955–60, Jul. 2009.

[15] L. B. Kratchman et al., "Design of a bone-attached parallel robot for percutaneous cochlear implantation." *IEEE Trans. Biomed. Eng.*, vol. 58, no. 10, pp. 2904–10, Oct. 2011.

[16] R. F. Labadie et al., "Clinical validation study of percutaneous cochlear access using patient-customized microstereotactic frames." *Otology & neurotology*, vol. 31, no. 1, pp. 94–9, Jan. 2010.

[17] J. T. Roland, "A model for cochlear implant electrode insertion and force evaluation: results with a new electrode design and insertion technique." *The Laryngoscope*, vol. 115, no. 8, pp. 1325–39, Aug. 2005.

[18] C. Todd et al., "Force application during cochlear implant insertion: an analysis for improvement of surgeon technique." *IEEE Trans. Biomed. Eng.*, vol. 54, no. 7, pp. 1247–55, Jul. 2007.

[19] J. Zhang et al., "Model and parameter identification of friction during robotic insertion of cochlear-implant electrode arrays," *Proc. 2009 IEEE Int. Conf. Robotics and Automation*, pp. 3859–3864, May 2009.

[20] G. Kontorinis et al., "Impact of the insertion speed of cochlear implant electrodes on the insertion forces." *Otology & neurotology*, vol. 32, no. 4, pp. 565–70, Jun. 2011.

[21] J. Pile and N. Simaan, "Characterization of Friction and Speed Effects and Methods for Detection of Cochlear Implant Electrode Tip Fold-over," in *Proc. 2013 IEEE Int. Conf. Robotics and Automation*, 2013, pp. 4394–4399.

[22] M. Miroir et al., "Friction force measurement during cochlear implant insertion: application to a force-controlled insertion tool design." *Otology & neurotology*, vol. 33, no. 6, pp. 1092–100, Aug. 2012.

[23] J. Pile, M. Y. Cheung, J. Zhang, and N. Simaan, "Algorithms and Design Considerations for Robot Assisted Insertion of Perimodiolar Electrode Arrays," in *Proc. 2011 IEEE Int. Conf. Robotics and Automation*, Shanghai, China, 2011, pp. 2898–2904.

[24] C. C. Finley et al., "Role of electrode placement as a contributor to variability in cochlear implant outcomes." *Otology & neurotology*, vol. 29, no. 7, pp. 920–8, Oct. 2008.

[25] R. J. S. Briggs et al., "Comparison of round window and cochleostomy approaches with a prototype hearing preservation electrode." *Audiology & neuro-otology*, vol. 11 Suppl 1, no. suppl 1, pp. 42–8, Jan. 2006.

[26] B. M. Verbist et al., "Consensus panel on a cochlear coordinate system applicable in histologic, physiologic, and radiologic studies of the human cochlea." *Otology & neurotology*, vol. 31, no. 5, pp. 722–30, Jul. 2010.

[27] M. Cosetti and J. T. Roland Jr, "Cochlear implant electrode insertion," *Operative Techniques in Otolaryngology, head & neck surgery*, vol. 21, no. 4, pp. 223–232, Dec. 2010.

[28] J. H. Noble, R. F. Labadie, O. Majdani, and B. M. Dawant, "Automatic segmentation of intracochlear anatomy in conventional CT." *IEEE Trans. Biomed. Eng.*, vol. 58, no. 9, pp. 2625–32, Sep. 2011.

[29] L. T. Cohen et al., "Improved and simplified methods for specifying positions of the electrode bands of a cochlear implant array." *American J. of Otology*, vol. 17, no. 6, pp. 859–65, Nov. 1996.

[30] M. H. Raibert and J. J. Craig, "Hybrid Position/Force Control of Manipulators," *J. of Dynamic Systems, Measurement, and Control*, vol. 103, no. 2, p. 126, 1981.

[31] T. Yoshikawa, "Dynamic hybrid position/force control of robot manipulators–Description of hand constraints and calculation of joint driving force," *IEEE J. on Robotics and Automation*, vol. 3, no. 5, pp. 386–392, Oct. 1987.

[32] J. Zhang et al., "Inroads Toward Robot-Assisted Cochlear Implant Surgery Using Steerable Electrode Arrays," *Otology & Neurotology*, p. 1, Jun. 2010.

[33] G. Kontorinis et al., "The effect of different lubricants on cochlear implant electrode insertion forces." *Otology & neurotology*, vol. 32, no. 7, pp. 1050–6, Sep. 2011.